Stem Cell Reports
Article

ISSCR

OPEN ACCESS

Imaging Transplanted Photoreceptors in Living Nonhuman Primates with Single-Cell Resolution

Ebrahim Aboualizadeh,[1,7] M. Joseph Phillips,[2,3,7] Juliette E. McGregor,[1,7] David A. DiLoreto, Jr.,[1,4] Jennifer M. Strazzeri,[1,4] Kamal R. Dhakal,[1] Brittany Bateman,[4] Lindsey D. Jager,[2] Kelsy L. Nilles,[2] Sara A. Stuedemann,[2] Allison L. Ludwig,[2] Jennifer J. Hunter,[1,4,5] William H. Merigan,[1,4,8] David M. Gamm,[2,3,6,8] and David R. Williams[1,5,8,*]

[1]Center for Visual Science, University of Rochester, Rochester, NY, USA
[2]Waisman Center, University of Wisconsin, Madison, WI, USA
[3]McPherson Eye Research Institute, University of Wisconsin, Madison, WI, USA
[4]Flaum Eye Institute, University of Rochester, Rochester, NY, USA
[5]The Institute of Optics, University of Rochester, Rochester, NY, USA
[6]Department of Ophthalmology and Visual Sciences, University of Wisconsin, Madison, WI, USA
[7]Co-first author
[8]Co-senior author
*Correspondence: david.williams@rochester.edu
https://doi.org/10.1016/j.stemcr.2020.06.019

SUMMARY

Stem cell-based transplantation therapies offer hope for currently untreatable retinal degenerations; however, preclinical progress has been largely confined to rodent models. Here, we describe an experimental platform for accelerating photoreceptor replacement therapy in the nonhuman primate, which has a visual system much more similar to the human. We deployed fluorescence adaptive optics scanning light ophthalmoscopy (FAOSLO) to noninvasively track transplanted photoreceptor precursors over time at cellular resolution in the living macaque. Fluorescently labeled photoreceptors generated from a $CRX^{+/tdTomato}$ human embryonic stem cell (hESC) reporter line were delivered subretinally to macaques with normal retinas and following selective ablation of host photoreceptors using an ultrafast laser. The fluorescent reporter together with FAOSLO allowed transplanted photoreceptor precursor survival, migration, and neurite formation to be monitored over time *in vivo*. Histological examination suggested migration of photoreceptor precursors to the outer plexiform layer and potential synapse formation in ablated areas in the macaque eye.

INTRODUCTION

In the case of severe retinal degenerations that destroy photoreceptors, a human pluripotent stem cell (hPSC)-based therapy that replaces lost photoreceptors is attractive because, if functional connections could be established between transplanted photoreceptor precursors and the rich variety of inner retinal circuits present in the primate retina, these circuits could potentially be restored to perform the diverse physiological functions they serve in the normal eye (Gasparini et al., 2018; Jayakody et al., 2015). Restoring vision at the photoreceptor level avoids the challenge that other approaches, such as epi-retinal electrical prostheses (Ghezzi, 2015) or optogenetics (Busskamp et al., 2012), face when the retinal circuitry is bypassed and the many ganglion cell classes, each specialized for a different function, are stimulated directly.

Robust protocols have been developed for the production of hPSC-derived photoreceptor precursors, primarily as an enriched cell type found within hPSC-derived retinal organoids (ROs) (Lakowski et al., 2018; Meyer et al., 2011; Phillips et al., 2014). While manufacturing physiologically functional differentiated photoreceptors from hPSCs has been well established *in vitro* (Phillips et al., 2018; Zhong et al., 2014), far less is known about their behavior *in vivo*, due to a number of technical hurdles. These include ensuring the long-term survival of photoreceptor precursors in the host environment, establishing a layer of light-sensitive cells of sufficient area and density to provide visual benefit, and neural integration of the photoreceptor precursors with the host retina (Santos-Ferreira et al., 2017; Singh et al., 2018).

Currently, histological methods can provide information about the impact of a given therapy at a microscopic spatial scale; however, this can only be performed at a single time point at the end of each experiment with each animal. Performing histology at multiple time points is costly in time, money, and the required animal numbers, especially in nonhuman primates. Furthermore, of the few transplantation studies that have been performed in nonhuman primates (Chao et al., 2017; McGill et al., 2018; Shirai et al., 2016; Tu et al., 2019), all have deployed conventional SLO or optical coherence tomography (OCT) imaging to evaluate transplantation outcomes, which lack sufficient resolution to assess the behavior of transplanted cells.

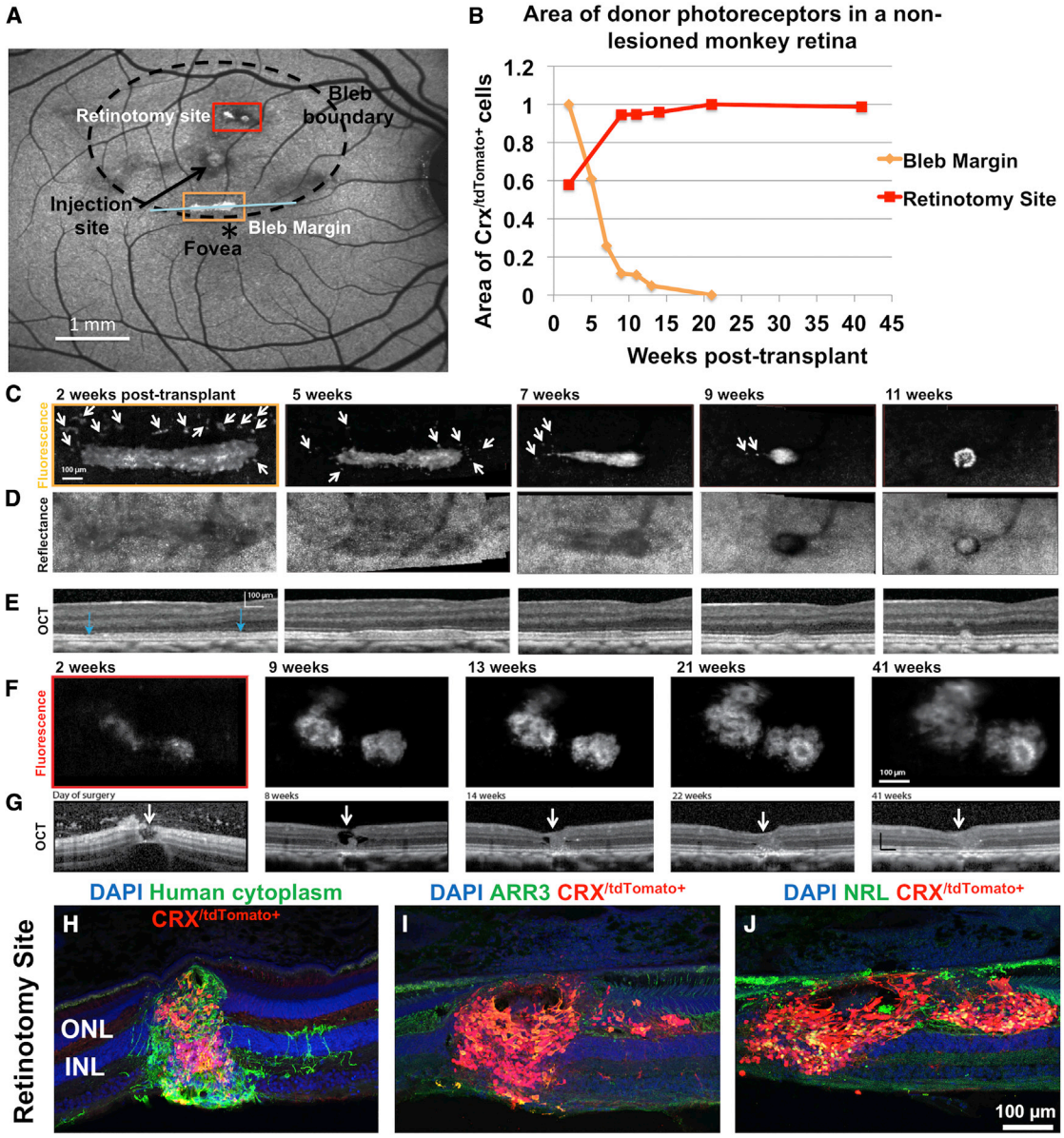

Figure 1. Long-Term Evaluation of Transplanted Photoreceptor Precursors in a Normal, Non-lesioned Monkey Retina

(A) Following transplantation, SLO imaging of the retina 4 weeks post transplant shows three regions with fluorescent cells, two at or near retinotomies associated with injection attempts, and one at the inferior aspect of the bleb. Bleb boundary (dotted circle) and injection site (black arrow) are shown. Retinotomy site refers to the incision created during failed attempts to raise a bleb.

(B) Quantification of two areas of transplanted photoreceptors using FAOSLO. There is a gradual loss of individual cells in the main cell cluster at the inferior margin of the bleb; however, at the retinotomy site there was an increase in the the area of the cell clusterfrom 2 to 9 weeks, followed by apparent stabilization up to 41 weeks post transplantation.

(C) FAOSLO imaging tracking a tdTomato labelled cell cluster at the inferior mergin of the bleb (yellow box in A) over an 11-week period. White arrows show loss of single cells and small clusters over time.

(D) NIR reflectance AOSLO imaging showed the photoreceptor mosaic in the same region as (C).

(E) OCT showed the axial changes in the transplant shown in (C) over time with blue arrows indicating the location of the cell cluster.

(F) FAOSLO images tracking a tdTomato labelled cell cluster at the retinotomy site (red box in A) over a 41-week period are shown.

(legend continued on next page)

Here, we show that these challenges can be largely overcome by supplementing histology with high-resolution, *in vivo* fluorescence imaging of individual cells with adaptive optics. Fluorescence adaptive optics scanning light ophthalmoscopy (FAOSLO) imaging (Gray et al., 2006; Rossi et al., 2017; Williams, 2011) reduces the need to euthanize large numbers of animals at various time points for histology and establishes a platform in which experimental manipulations can be studied more easily.

The nonhuman primate model is needed because the monkey has a fovea and human-like visual perception with a similar immune system to humans. Moreover, the use of nonhuman primates could mitigate risk to patients in subsequent clinical trials (Regenberg et al., 2009). While inherited models of retinal degeneration have recently been identified in nonhuman primates (Moshiri et al., 2019; Peterson et al., 2019), at present there is no readily available genetic primate model of retinal degeneration. In this study, we used a recently developed model of selective photoreceptor ablation by using femtosecond pulses of near infrared (NIR) light onto the retina with adaptive optics (Dhakal et al., 2020). This method of photoreceptor ablation leads to minimal disruption of the surrounding tissue, including the retinal pigment epithelium (RPE).

To image transplanted photoreceptor precursors with single-cell resolution *in vivo*, ROs from a previously described hESC-CRX$^{+/tdTomato}$ photoreceptor reporter line (Phillips et al., 2018) were dissociated and transplanted in the subretinal space of nonhuman primates. FAOSLO imaging was then used to track photoreceptor precursor survival, migration, and morphology over time. Only cells that re-aggregated after transplantation remained viable in the normal, undamaged retina. However, these cells remained confined to the subretinal space and did not integrate, with a noted exception at the injection site. By comparison, transplanted cells at ultrafast laser lesion sites were shown to migrate into the host retina and demonstrated potential for synaptic connectivity. With FAOSLO, we were able to ascertain the behavior of photoreceptor precursors in living nonhuman primates and image donor cells with single-cell resolution, including fine neurites, for the first time.

RESULTS

Long-Term Evaluation of Photoreceptor Precursors in the Subretinal Space of Normal Monkeys

To facilitate single-cell imaging *in vivo*, hESC-CRX$^{+/tdTomato}$ optic vesicles were fully dissociated and transplanted in the subretinal space of two normal, non-lesioned nonhuman primates to optimize the surgical approach and imaging techniques, and to evaluate long-term cell survival.

Monkey 1 was followed for 41 weeks (Figure 1). Following transplantation, three regions with fluorescent cells were present, two at or near retinotomies associated with injection attempts, and one at the inferior aspect of the bleb (Figure 1A). These regions were followed with FAOSLO imaging and the area of fluorescent photoreceptor precursors was quantified over time. Two of these areas showing differential transplant survival are shown in Figure 1.

The aggregation of cells at the inferior aspect of the bleb was presumably gravity driven, as the monkey head was positioned upright immediately post surgery for OCT imaging. Photoreceptor precursors at the inferior aspect of the bleb showed gradual loss between 2 and 21 weeks post transplant (Figures 1B and 1C). In this region, the majority of single cells or smaller cell clusters were lost by week 5 (Figure 1C, arrows), with a nearly 90% reduction in transplant area by week 11. Furthermore, the morphology of the remaining photoreceptor precursor aggregate at 11 weeks resembled a rosette-like structure (Zhang et al., 2001), suggesting lack of integration with the host. AOSLO NIR reflectance imaging (Figure 1D) and OCT (Figure 1E) confirmed that the host retina in this region was not permanently affected by the presence of donor cells and that the host photoreceptor mosaic returned to normal once the donor cells were gone.

By contrast, at the retinotomy site created during failed attempts to raise a bleb in a non-vitrectomized eye, the area of fluorescent cells gradually increased from 2 to 9 weeks after transplantation and then remained approximately stable afterward (Figures 1B and 1F). OCT taken on the day of surgery showed a retinotomy created during the surgical procedure. In the vitreous it is possible to see effluxed cells that have escaped the subretinal space through the hole. Over time the size of the transplant

(G) OCT showing axial changes in the transplant shown in (F) at the retinotomy site a 41 week period. White arrows show the hole that was created at the retinotomy site. As shown, significant cell efflux was observed, which we attribute to raising the bleb and injecting donor cells simultaneously in this case.

(H–J) Immunohistochemistry at 41 weeks post transplant demonstrated the presence of transplanted cells (human cytoplasm+), including CRX$^{/tdTomato+}$ photoreceptors, which filled the retinotomy site. (I and J) Transplanted photoreceptors matured *in vivo* to express cone (I) and rod (J) markers.

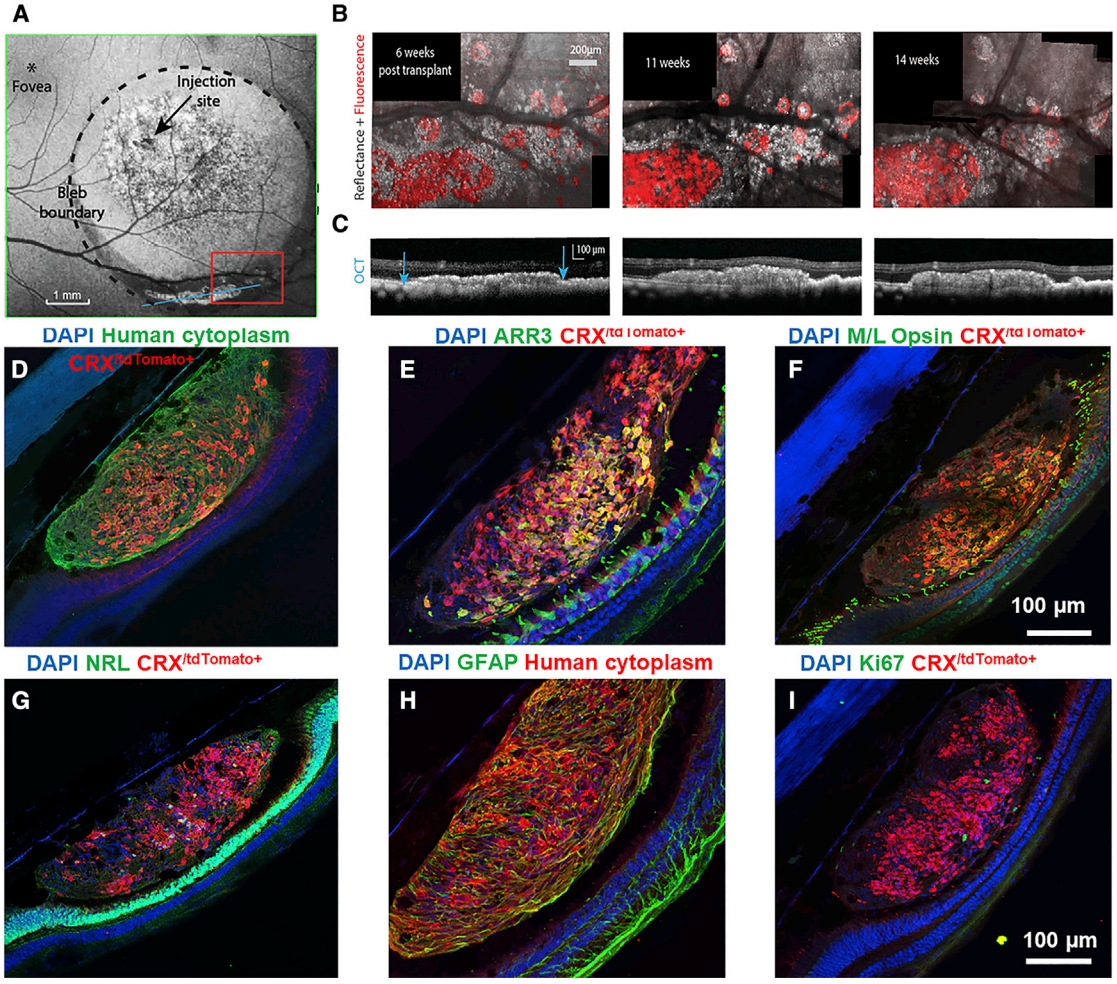

Figure 2. Photoreceptor Precursors in a Non-lesioned Retina Remained Confined to the Subretinal Space

(A) A blue autofluorescence SLO image of the bleb and transplanted cells is shown. Autofluorescence from disrupted RPE can be seen in the central bleb as well as tdTomato fluorescence from the transplanted cells at the inferior margin of the bleb. The region bounded by the red box was imaged using FAOSLO and AOSLO NIR reflectance imaging for 14 weeks.

(B) Merged fluorescence (red) and NIR reflectance (gray) AOSLO images taken at 6, 11, and 14 weeks post transplant are shown.

(C) OCT of the region containing the transplanted cells along an axis corresponding to the blue line shown in (A) is shown.

(D–I) CRX$^{/tdTomato+}$ cells always co-labeled with a human cytoplasm-specific antibody, confirming that these cells were of human origin. Additional retinal cell types from the dissociated organoids were also present (i.e., human cytoplasm+/CRX$^{/tdTomato}$-cells). Photoreceptor precursors demonstrated expression of cone (E and F) and rod markers (G), Some human cytoplasm+/GFAP^{+} glial cells were also present within the cell cluster (H), while proliferative cells were minimal (I).

increased and the retinotomy was sealed by 21 weeks post transplant (Figure 1G, arrows). FAOSLO showed that the transplant in this region was composed of multiple rosette-like structures. Histology at 41 weeks confirmed the presence of donor photoreceptors at the injection site (Figures 1H–1J). Presumably, the hole created by the injection cannula either trapped cells at the time of the injection or allowed cells to migrate into the hole post injection.

In a second monkey, *in vivo* imaging once again showed a region of photoreceptor precursors localized within the inferior portion of the bleb (Figure 2A). In this case the transplant was stable for the 14-week period of AOSLO imaging and survived until the 29-week euthanasia point (Figure 2B). A large aggregate of cells and rosette-like structures was observed. OCT confirmed a thickened transplant region along the inferior aspect of the bleb (Figure 2C, blue arrows). Simultaneous NIR reflectance AOSLO and FAOSLO confirmed that this region contained viable donor photoreceptors (Figure 2B).

Histological analysis at week 29 indicated that transplanted cells in this region were primarily photoreceptors (Figures 2D–2I); however, human cytoplasm+/GFAP+

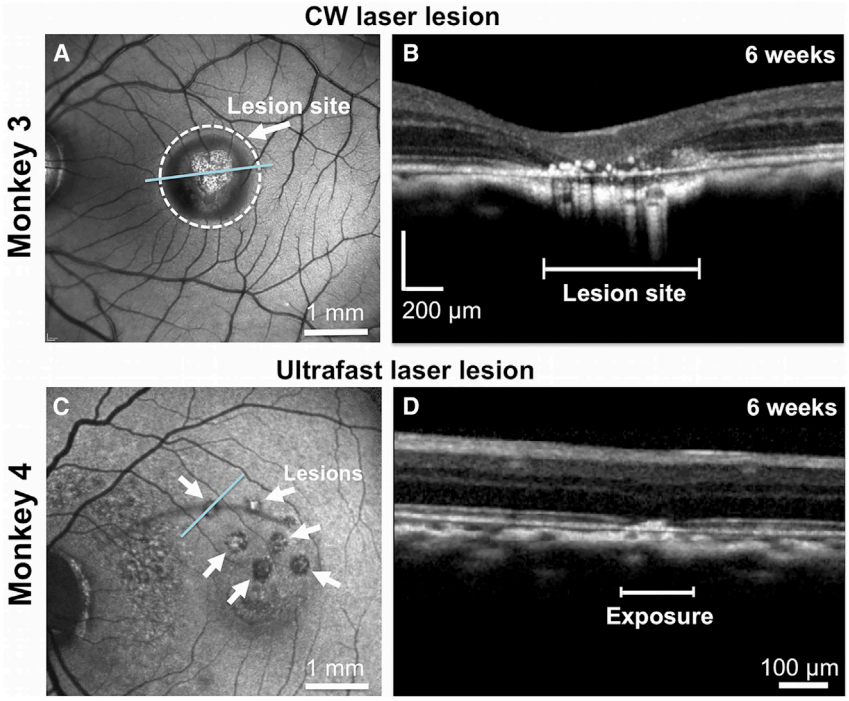

Figure 3. Evaluation of the Retinal Impact of Exposure to a CW Laser and an Ultrafast Laser Using SLO and OCT

(A and B) Conventional SLO (A) and a spectral-domain OCT scan (B) of a monkey retina ablated with a CW laser at 6 weeks post exposure. At the lesion site, there is complete ablation of the outer retina with apposition of the inner plexiform layer to the RPE. The RPE is irregular with overlying scattered hyperreflective foci. OCT scan was acquired in the area designated by the blue line in (A).

(C and D) SLO (C) and a spectral-domain OCT scan (D) of a monkey retina ablated using an ultrafast laser with adaptive optics at 6 weeks post exposure. OCT imaging shows localized disruption within the outer limiting membrane and the outer nuclear layer. The linear dimension of an exposure area is shown on the OCT scan. OCT was acquired across the blue line in (C). White arrows in (C) highlight the pattern of ultrafast laser lesions.

Muller glia were also present and may have contributed to donor cell survival in the subretinal space (Figure 2H). Subsets of photoreceptor precursors matured to express cone and rod markers in both monkeys 1 and 2 (Figures 1I, 1J, and 2E–2G). Proliferative (Ki67+) cells were minimal after long-term transplantation (Figure 2I). Despite the long-term survival of the cells in monkey 2, there was no evidence of integration with the intact neural retina of the host and the cells remained confined to the subretinal space.

Selective Photoreceptor Ablation Using High Intensity, Ultrafast, Light Pulses Delivered via Adaptive Optics

The use of a CW laser to destroy photoreceptors (Strazzeri et al., 2014) caused three undesirable effects: retinal adhesion, destruction of the RPE, and a strong immune response (Figure S1). Following a preliminary attempt (see Note S3), we decided not to pursue this approach further for transplantation studies, although it was possible that we could have reduced these problems with a lower light exposure. Instead, we adopted a laser lesion method recently developed in our laboratory and described in detail in Dhakal et al. (2020). Selective photoreceptor ablation was observed after exposing host photoreceptors to ultrafast pulses of light delivered using the adaptive optics system. SLO and OCT imaging of the CW lesion (Figures 3A and 3B, arrow) and AO ultrafast laser lesion (Figures 3C and 3D, arrows) at 6 weeks post exposure are shown. OCT imaging demonstrated that disruption in the AO ultrafast lesions was confined largely to the photoreceptor layer, while in the CW case, retinal layers neighboring the lesion appeared compromised. Localizing damage to the photoreceptor layers is critical because disruption of the RPE affects photoreceptor support and can compromise the blood-retinal barrier, and damage to the inner retina impedes functional circuit restoration. This model was successfully deployed in monkeys 4 and 5 for transplantation studies with no adhesion of retina to the RPE, far less apparent disruption of the RPE blood/retinal barrier, and the presence of very few T- and B-positive cells in the retina.

FAOSLO Imaging of Photoreceptor Precursors in the AO Ultrafast Nonhuman Primate Model

Photoreceptor survival and integration were assessed in two monkeys following host photoreceptor ablation using AO ultrafast laser lesions (monkeys 4 and 5). Monkey 4 was injected at both lesioned and non-lesioned areas for a direct comparison and followed for 12 weeks, while a second laser-lesioned monkey (monkey 5) was injected only at the lesion site and followed for 5 weeks to examine long- versus short-term cell survival and integration. Both animals received a vitrectomy which afforded greater control over bleb formation and the removal of effluxed cells from the eye. Given that transplanted cells settled at the inferior aspect of the bleb in previous cases (M1-M3), these two monkeys were positioned prone for 3–4 h post implantation to tamponade the injection site, which resulted in a

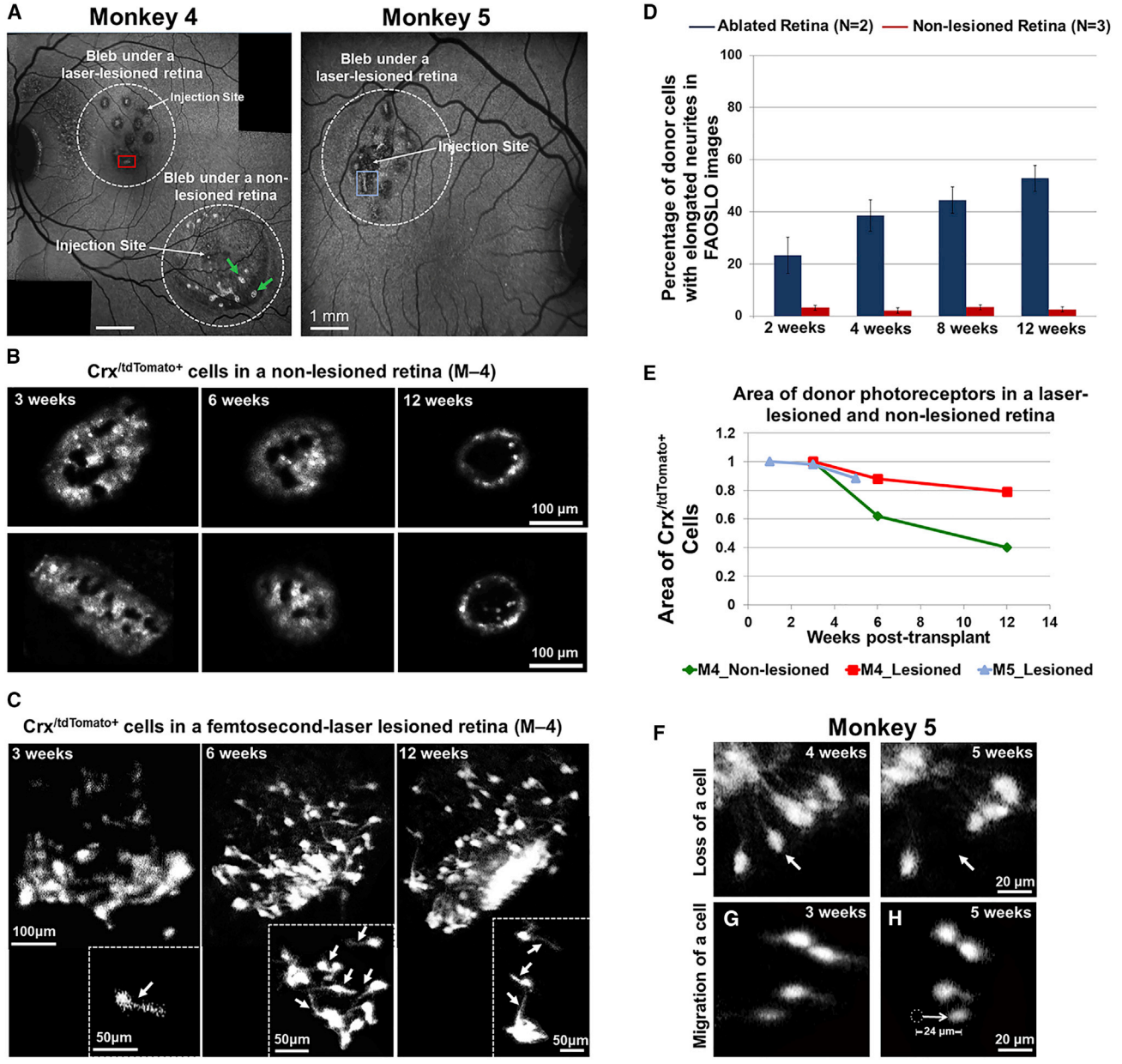

Figure 4. FAOSLO Imaging of Photoreceptor Precursors in the AO Ultrafast Nonhuman Primate Model

(A) SLO images of photoreceptor precursors in monkeys 4 and 5, 3 weeks post transplantation are shown. Monkey 4 was tracked with *in vivo* FAOSLO imaging for 12 weeks and monkey 5 was tracked for 5 weeks. For a direct comparison within the same eye in monkey 4, one transplant was performed in the lesioned area and one was performed in a non-lesioned area. Monkey 5 received a transplant into a lesioned area.

(B and C) FAOSLO images of transplanted cells in a non-lesioned retina (B) and an AO ultrafast-laser-lesioned retina are shown (C) at 3, 6, and 12 weeks post transplant. (B) FAOSLO imaging of two cell clusters in a non-lesioned retina (green arrows in A) showed loss of donor cells over time. (C) By comparison, transplanted cells in the lesioned area extended neuronal processes over time are shown (see also Figure S1). Fine neurites could be resolved on individual photoreceptor precursors in this region with FAOSLO (white arrows).

(D) Area of transplanted cells in two monkeys and both blebs were quantified, showing pattern of cell loss in both ablated and non-lesioned retinas.

(E) The percentage of single cells with extended neurites in the lesioned retinas (N = 2) varied between 22% and 52%; however, in non-lesioned retinas (N = 3), this percentage was less than 8% over a 12-week period.

(legend continued on next page)

more even distribution of cells within the bleb. Steps were taken to ensure that tdTomato fluorescence specifically labeling the donor cells was distinguished from host autofluorescence (see Note S4) in subsequent FAOSLO imaging.

Post-operative *in vivo* images of photoreceptor precursors in monkeys 4 and 5 are shown in Figure 4. SLO imaging at 3 weeks post transplant showed clusters of transplanted cells within the bleb (Figure 4A, white circles). FAOSLO imaging of two cell clusters in the non-lesioned bleb in monkey 4 (green arrows in Figure 4A) demonstrated pronounced cell loss between 3 and 12 weeks, including preferential cell loss in the center of the cell clusters (Figure 4B). However, in the bleb containing the lesions, there was evidence of persistent clusters of photoreceptor precursors from 3 to 12 weeks (Figure 4C; red box in Figure 4A).

Striking differences were observed in the morphology of donor cells in non-lesioned versus lesioned regions. In non-lesioned areas, there was little to no evidence of neural processes extending from transplanted cells (Figure 4B, see also Figures 1–3). Also, transplanted cells appeared as large clusters with few individual cells. Conversely, neurite formation was pronounced in numerous individual photoreceptor precursors located in ablated regions (Figure 4C, arrows; Figure S2). Figure 4D shows a greater percentage of individual photoreceptor precursors with neurites in lesioned retinas as opposed to non-lesioned retinas at multiple time points.

To quantify photoreceptor precursors survival, the area of transplanted cells in laser-lesioned and non-lesioned retinas was measured using FAOSLO imaging over the tracking period (Figure 4E). The total area of transplanted cells in the non-lesioned bleb in monkey 4 decreased by ~40% after 6 weeks and by ~60% at 12 weeks post transplant (Figure 4E). However, the area of transplanted cells in the lesioned area in monkey 4 showed a much smaller reduction (only ~20% after 6 weeks), which remained almost unchanged up to 12 weeks. In monkey 5, the area of transplanted cells decreased by less than 20% between 1 and 5 weeks post transplant.

In monkey 5, FAOSLO revealed the occasional loss of an individual photoreceptor precursor (Figure 4F, arrows). Single cell migration over a distance of 24 μm in a 2 week time period, was also observed as shown in Figures 5G and 5H.

In both monkeys 4 and 5, some transplanted cells settled within the middle of the lesion (Figure S2 and Note S4) and single photoreceptor precursors demonstrated prominent neuronal processes, suggesting the potential contact between donor photoreceptors and host bipolar cells in ablated retinas.

Histological Examination of Photoreceptor Precursor Integration and Differentiation

Histological analysis in the ablated areas of monkeys 4 and 5 showed few T cells (CD3+) or B cells (CD20+) near transplanted cells (Figures 5A and 5B; monkey 4 shown). Some transplanted cells in monkey 4 were elongated in the same direction as the host photoreceptors (Figure 5B, inset). A similar reduced immune response was noted in the non-lesioned area of monkey 4 (Figure S3). In blebs that contained an AO ultrafast lesion, photoreceptor precursors migrated from the subretinal space to the host outer plexiform layer (OPL) in both monkeys 4 and 5, presumably through entry sites provided by the laser lesions (Figures 5C–5I). As evidence of this phenomenon, transplanted cells were routinely found occupying the ablated region in the host outer nuclear layer (ONL) (Figures 5C, 5F, and 5H), while adjacent sections had numerous photoreceptor precursors present in the host OPL (Figures 5D, 5E, 5G, and 5I). These ectopic photoreceptor precursors extended processes, often directed toward the inner nuclear layer (INL). The fact that these findings were nearly identical in both monkeys 4 and 5 (collected at 12 and 5 weeks, respectively) suggested that migration and neurite formation occurred within the first 5 weeks post transplant. Corresponding FAOSLO imaging of the same area pre-euthanasia confirmed the ability of this imaging technique to detect neurite formation in the living animal (Figure 5J, arrows). The majority of transplanted cells (human cytoplasm+) found in the OPL were photoreceptors, suggesting preferential migration of photoreceptor precursors (versus other donor retinal cell types) toward the host INL. In non-lesioned retina, donor cells remained in the subretinal space with no evidence of human cytoplasm+ cells in the host ONL or OPL. Furthermore, the morphology of the photoreceptor precursors was quite distinct from that of host photoreceptors.

Immunohistochemical examination of photoreceptor precursor integration and differentiation is shown in Figures 6A–6H. Some photoreceptor precursors matured *in vivo* to express M/L opsin (Figure 6A). Neurites from photoreceptor precursors contacted host second-order neurons, including G0α+ ON bipolar cells (Figure 6B, arrows), PKCα+ bipolar cells (Figure 6C, arrows), and CALB1+ horizontal and bipolar cells (Figures 6E and 6F). In addition,

(F–H) (F) Single-cell tracking using FAOSLO imaging showed loss of a single photoreceptor precursor between 4 and 5 weeks post transplant (white arrows) and migration of a different photoreceptor precursor over a 2-week period (G). White dotted circle in (H) shows the original position of a single cell at 3 weeks and the white arrow shows the direction of migration. Errors bars represent standard error and N represents number of animals.

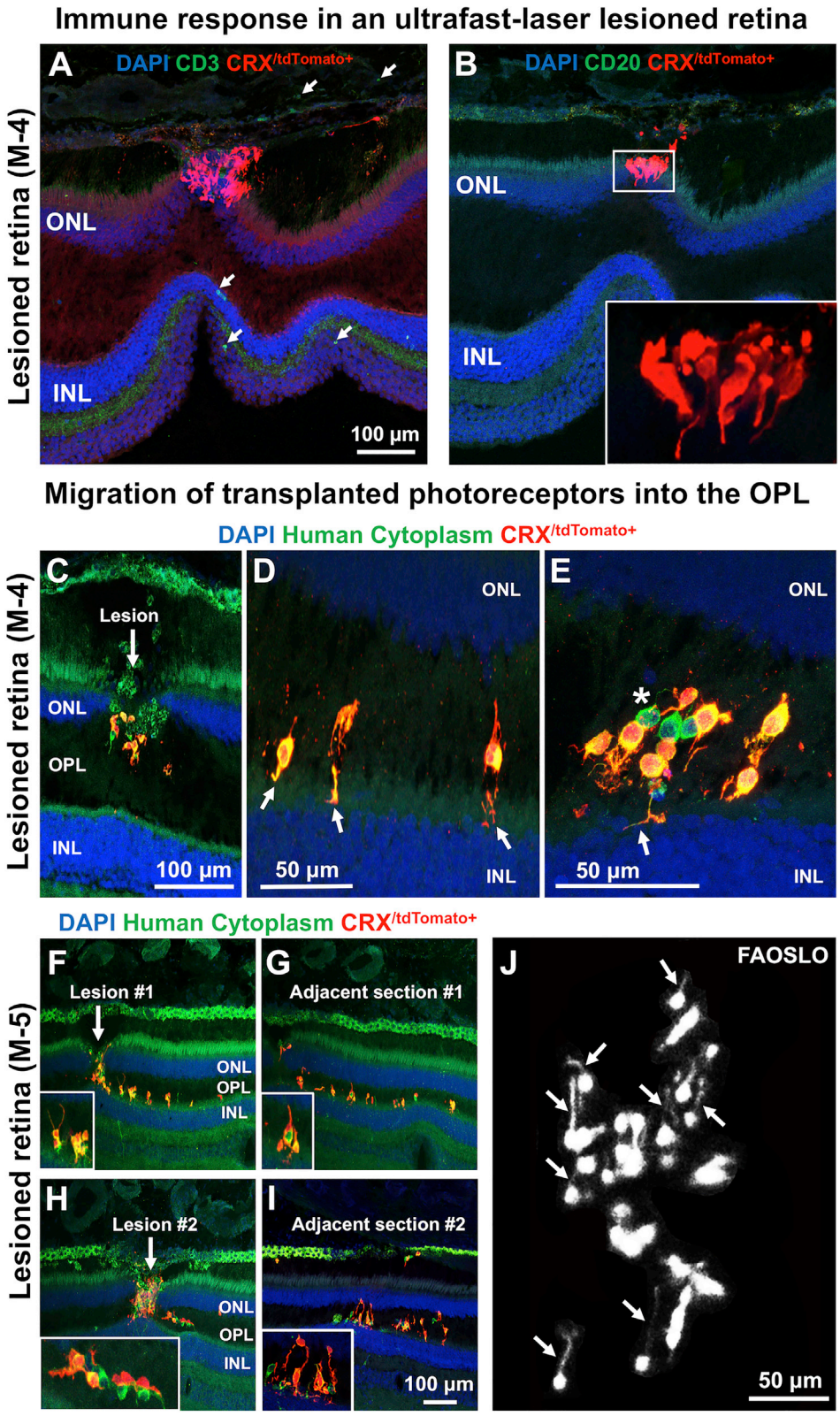

(legend on next page)

photoreceptor precursors expressed the presynaptic marker synaptophysin (Figure 6D, arrows). While expression of synaptophysin in photoreceptor precursors was disorganized in cells away from the host OPL, processes close to the host INL had pronounced expression of synaptophysin in putative axonal terminals (Figures 6G and 6H), suggesting the potential for synapse formation. While the potential for synaptogenesis between donor cells and host bipolar cells in nonhuman primates is promising, further studies are required to determine whether they are functional. Importantly, no teratomas were noted in any of the transplanted nonhuman primates.

DISCUSSION

In this study, we utilized FAOSLO to image transplanted hESC-CRX$^{+/tdTomato+}$ photoreceptor precursors at single-cell resolution in the living eye. Before this study, little was known regarding the dynamic nature of transplanted cells in living retina at cellular resolution, most of which has been inferred from OCT or histology after euthanasia (da Cruz et al., 2018; Kashani et al., 2018; Sharma et al., 2019). Using FAOSLO, we tracked the survival, migration, and neurite outgrowth of individual fluorescent photoreceptor precursors in the living monkey eye. Postmortem histology confirmed these findings, and demonstrated the differentiation of photoreceptor precursors into a rod or cone cell fate. In ablated retinas, photoreceptor precursors migrated into the host OPL and showed the potential to form synapses with host bipolar and horizontal cells.

Comparison between the AO Ultrafast Laser Ablation and CW Laser Ablation

We used a recently developed method of ablating photoreceptors to create precise and reproducible scotomas in the macaque peripheral retina suitable for transplantation studies. Initially we attempted to use a CW laser to damage host photoreceptors; however, this resulted in adhesion of retina, precluding a safe detachment of retina from the adherent RPE during transplantation. In addition, the higher laser power led to RPE cell death and loss of the blood-retinal barrier (Figure S1), providing an entry site for B cells and T cells to flood into the subretinal space. Our results with CW lesions should not be construed as the best possible outcome that might eventually be achievable with that approach, but it did inspired us to develop another approach for which there is a strong theoretical basis for improved localization of the lesion (Jain et al., 2008; Vogel and Venugopalan, 2003). The AO ultrafast ablation method, which combines adaptive and nonlinear optics, abruptly destroys host photoreceptors with minimum damage to surrounding tissues, making it a useful tool for creating localized lesions in the outer retina for use in nonhuman primate vision restoration studies. However, this model does have the limitation that it does not replicate all of the sequential, time-dependent consequences that follow from inherited photoreceptor degenerative diseases.

Evidence against Cytoplasmic Exchange of Fluorescence between Donor and Host

Previous mouse studies reported an inverse correlation between the integrity of the outer limiting membrane and the integration of donor photoreceptors (Barber et al., 2013; Pearson et al., 2010; West et al., 2008). However, the extensive transplanted photoreceptor integration seen in previous allogeneic mouse studies has now been shown to arise primarily from cytoplasmic transfer of fluorophore proteins between donor photoreceptors in the subretinal space and the remaining host photoreceptors (Ortin-Martinez et al., 2017; Pearson et al., 2016; Santos-Ferreira et al., 2016; Singh et al., 2016) forcing a revaluation of this previous work. There are several lines of evidence to indicate

Figure 5. Immunohistochemical Examination of Photoreceptor Precursors in the AO Ultrafast-Lesioned Retina

(A and B) Histological examination of transplanted cells in an ultrafast-lesioned retina in monkey 4 is shown. In this model, very few anti CD3 T cells (A) and anti CD20 B cells (B) were noted (see also Figure S2). Transplanted cells in higher magnification are shown in the inset.

(C) In monkey 4, histology at 12 weeks showed that transplanted photoreceptors had migrated into the OPL through the laser lesion site.

(D) Some donor cells extended neurites toward the INL through the entry site provided by laser lesions (white arrows).

(E) Additional cells that had migrated to the OPL and contacted the host INL by extending neurites are shown (White arrow). Asterisk in (E) shows human non-photoreceptors.

(F) In monkey 5, similar migration of transplanted photoreceptor precursors into the host OPL was noted at the ablation site within a shorter period of time (5 weeks, cells are shown at higher magnification in the insets).

(G) The Adjacent section also showed transplanted cells that migrated to the OPL through the laser lesions and extended neuronal processes.

(H) Migration of donor photoreceptors into the OPL through the second lesion site is shown.

(I) Similarly, the adjacent section showed migration of donor cells to the OPL and extension of neuronal processes (higher magnification images are shown in the insets).

(J) FAOSLO imaging at the same retinal location, 1 week before euthanasia, showing the capability of FAOSLO to resolve fine neurites extending laterally *in vivo*.

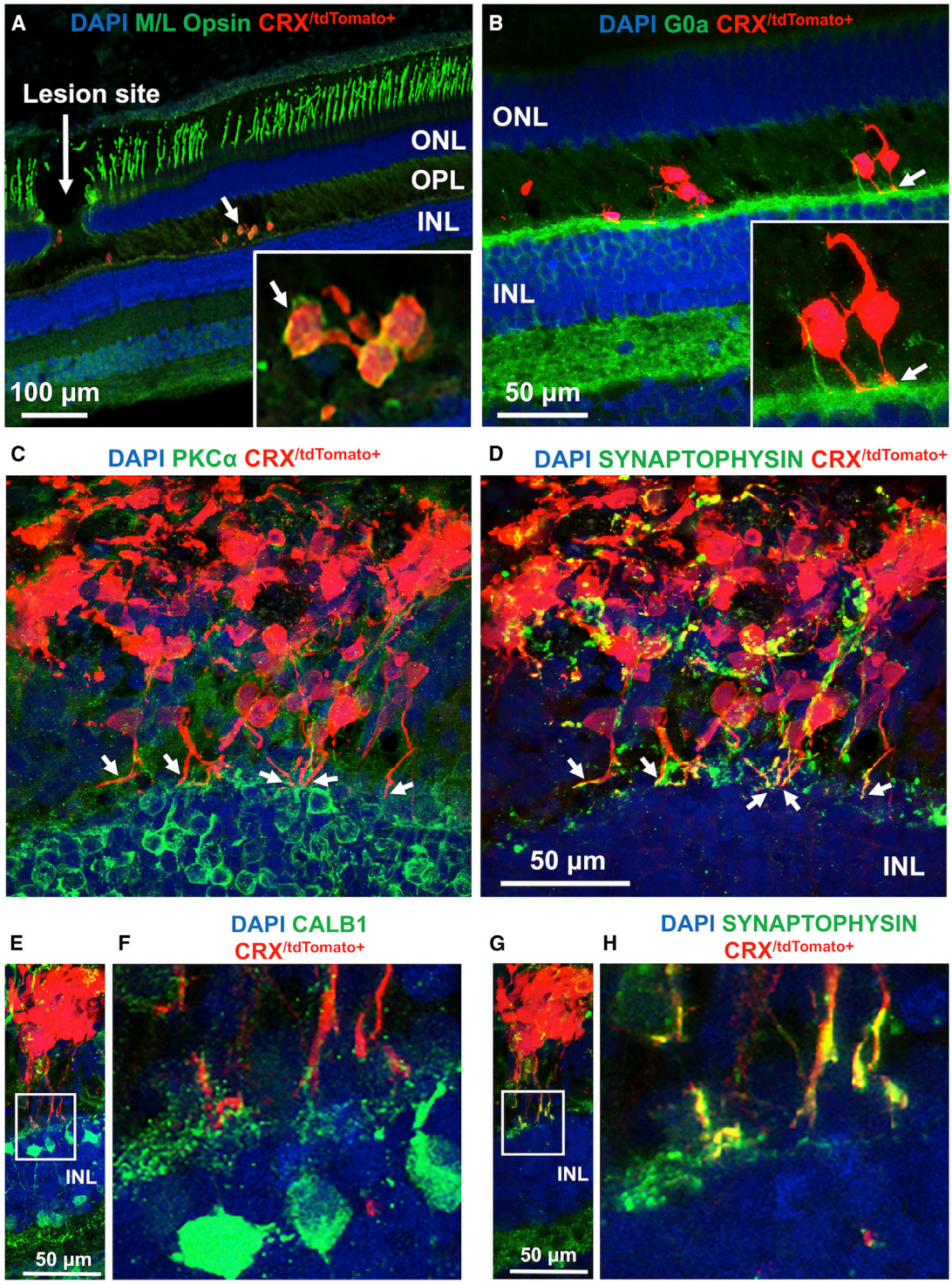

Figure 6. Immunohistochemical Examination of Photoreceptor Precursor Integration and Differentiation

(A) Some migratory transplanted photoreceptor precursors matured *in vivo* to express M/L opsin.

(B) Neurites from transplanted cells were in contact with host second-order neurons, including GOα+ ON bipolar cell dendrites.

(legend continued on next page)

that cytoplasmic material exchange did not occur in our xenograft studies. First, in areas of a non-lesioned retina where donor photoreceptor precursors remained confined to the subretinal space, there were no underlying tdTomato+ or human cytoplasm+ cells in the host ONL. Second, transplanted photoreceptor precursors that migrated into the host retina in laser-lesioned areas were almost exclusively found ectopically in the host OPL, where no host photoreceptors are present. Third, there is currently debate in the field about whether cytoplasmic material exchange may primarily be a transient phenomenon. Mouse studies have demonstrated material transfer 2–3 weeks post transplantation (Ortin-Martinez et al., 2017; Santos-Ferreira et al., 2016; Singh et al., 2016); however, it is possible that these proteins are short lived. If this were the case, the data in our study would be unlikely to be affected as *in vivo* imaging and histology was performed several weeks to months after transplantation. Finally, the morphology of transplanted photoreceptor precursors was very different from the structure of host photoreceptors. When cytoplasmic exchange occurs in mice, those cells are morphologically indistinguishable from surrounding host photoreceptors. As such, it is unlikely that cytoplasmic transfer occurred in our human-to-monkey transplants.

Survival of Photoreceptor Precursors Transplanted into the Subretinal Space

FAOSLO imaging allows us to track differential survival of transplanted cells. Although some imaging tools, such as OCT provide high axial resolution, unspecific morphological information about the transplant may be misinterpreted without fluorescence imaging (McGill et al., 2018). Figures 2B and 2C show OCT scans through the region imaged with AOSLO presented at the same lateral scale. The OCT data show a thickened region, but lack the specificity to show to what extent this cell mass contains viable photoreceptor precursors. The FAOSLO images show that this region is not the homogeneous mass of CRX/^{tdTomato}-positive cells that might OCT suggest, but rather there are regions where CRX/^{tdTomato}-positive cells are sparser and are forming rosette-like structures. There are non-fluorescent regions within the thickened region that are hyperreflective in the NIR and may represent cells that are no longer viable or represent damaged host RPE. These regions merit further investigation. OCT in conjunction with the specificity afforded by FAOSLO allows a more complete understanding of the status of the implant.

When donor cells remained confined to the subretinal space, an initial loss of single cells was observed with the last cells to disappear being those in clusters, which often developed a rosette-like morphology. Quantification of the area of these cells suggested that the cell loss was between 60% and 90% (M1, M3, and M4) at 12 weeks post transplant. By contrast, in ablated retinas, donor cells that migrated to the OPL and were in contact with bipolar cells experienced less than 20% cell loss at 12 weeks (M4). The rate of cell loss in (M5) was also less than 20% albeit over the shorter 5-week tracking period. However, we noted an exception in which transplanted cells in the non-ablated retina that were sequestered to the subretinal space with no integration, survived up to 29 weeks post transplant (M2). Furthermore, in three animals (M1, M2, and M3), at the injection sites, transplanted cells survived until the end of the tracking period, 41, 29, and 11 week, respectively.

At present, the factors that govern donor cell survival are unknown. Although an immune response could be one explanation for the cell loss, as suggested in monkey 3, other nonimmune-based mechanisms may also be involved, including access to appropriate trophic support, developmental cues, and the appropriate biochemical environment. Our attempts to evaluate the immune response at the end of the observation period are shown in Figures 5, S1, and S3, and are discussed in Note S5. So far we have been unable to see a clear correlation between the immune response at that single time point and the rate of cell loss. The development of a method to track the immune response locally in the retina throughout the observation period could help resolve this question.

Outer Segment Differentiation

Histology in both non-lesioned and ablated retinas, showed that subsets of transplanted photoreceptor precursors expressed rod and cone genes at the point of euthanasia, including M/L opsin at cell differentiation days 364 (M1), 297 (M2), and 174 (M4), respectively. Although the expression of rod and cone genes as well as cone photopigment by differentiated photoreceptor precursors is promising, there was little evidence of the development of the classical photoreceptor morphology, such as discs replete with photopigment and stacked in the outer segment waveguide (Figure 6B). Because they lack this structure,

(C and D) Some donor photoreceptor precursors extended axons toward host bipolar cells (PKCα+, C) and expressed the presynaptic protein marker (synaptophysin) (D). While expression of synaptophysin in transplanted cells was disorganized in cells away from the host OPL, processes close to the host INL had pronounced expression of synaptophysin in putative axonal terminals.
(E–H) Some photoreceptor precursors contacted host second-order neurons, including CALB1+ horizontal and bipolar cells (E and F) and expressed synaptophysin (G and H). The white squares in (E) and (G) are shown magnified in (F) and (H), respectively.

the donor cells we observed were almost certainly much less sensitive to light than normal receptors. However, it has also been shown that photoreceptors in disease models that lack fully formed outer segments can still respond to light and support useful vision (Thompson et al., 2014).

Previous authors have transplanted hESC-derived retinas (not only the photoreceptor precursor fraction) into nonhuman primate retinas that had retinal degeneration induced by cobalt chloride administration or full-thickness laser burns (Shirai et al., 2016). That study reported the development of photoreceptor outer segments and opsins within rosette structures that did not integrate with the host RPE. Outside of rosettes, photoreceptors remained immature. Whether it will ultimately be possible to create conditions in a mature primate that allow the formation of the complex normal morphology that ordinarily occurs during development, including for example integration with the RPE as well as Muller cells, remains to be seen.

Behavior of Photoreceptor Precursors in Regions of Photoreceptor Ablation

In ablated retinas, we observed individual photoreceptor precursors often formed long neurites that could be seen with the FAOSLO *in vivo* as well as with postmortem histology. In monkey M5 we observed approximately 20% of individual cells had neurites as early as 1 week post transplant, while >50% of cells extended neurites by 12 weeks. An increase of the individual photoreceptor precursors in the FAOSLO images over time might be due to either an improved optical quality of the eye over time after surgery that provided superior imaging resolution or the actual increase of single cells that migrated from cell clusters toward the lesion site and eventually to the OPL. We were not able to assess the temporal sequence of neurite outgrowth and migration because both were largely complete by the first imaging session, which was performed at least 1 week post transplantation. *In vivo* imaging of processes was facilitated by the use of a narrow emission filter that excluded RPE autofluorescence, enhancing the contrast of the relatively dim processes.

In regions of photoreceptor ablation, we observed that transplanted photoreceptors often extended neurites containing presynaptic proteins toward the host INL and were found juxtaposed to dendrites from second-order bipolar and horizontal cells. These promising findings may be due to any of a number of causative factors, including enhancement of the immune suppression regimen, a higher number of transplanted cells, improvements in the selective laser ablation technique, and the introduction of a vitrectomy step before transplantation. Limits on the numbers of large animals that can be devoted to these studies constrained our ability to evaluate the impact of each factor individually in this study. However, longitudinal tracking of photoreceptor precursors transplanted into two blebs raised in the same eye, one under regions of ablated retina and the second under a non-ablated region of retina provided a more direct comparison where the number of cells delivered to the eye, immune suppression, and delivery method were as similar as possible. Consistent with data from other monkeys this experiment showed that donor cell migration and maturation were associated with regions of photoreceptor ablation.

The correlation between photoreceptor ablation and transplanted photoreceptor precursors preferentially extending neurites could have arisen because these areas offered a path to integration with the host retina, but there are several alternative explanations for this observation that cannot be discounted. It is possible that this phenomenon is specific to our ablation technique, for example, the ultrafast laser may induce cytokine secretion or promoting neurite growth in transplanted cells or that neurite formation is a stress response of transplanted cells in this host environment. This method of photoreceptor ablation may not induce gliosis which may be advantageous for neurite formation relative to other ablation techniques or may provoke changes in RPE cells that are beneficial. The imaging technique described in this paper could be applied to investigate these issues further, including undertaking photoreceptor transplantation studies in models of inherited retinal disease, which would allow comparison of neurite formation in disease versus injury models.

Donor cell efflux was a challenge in all animals making it impossible to know exactly how many cells were delivered into the subretinal space regardless of the intended number injected into the eye. In monkeys 4 and 5, where we used vitrectomy approach meaning that any cells that effluxed back into the vitreous could be removed during surgery, this strategy prevents vitreous cell impacting vision and AOSLO imaging and would likely be used for patients. Improvements, such as optimizing the volume of the bleb before injection of cells and adjusting the speed of transplant delivery could be explored to minimize donor cell efflux to achieve maximum cell retention.

This study demonstrates that it is possible to detect photoreceptor migration and neurite extension in the living primate eye. Imaging transplanted photoreceptor precursors with single-cell resolution provides a platform for accelerating photoreceptor replacement therapy by improving the understanding of donor cell behavior in the living eye. The fluorescence imaging technique described here provided feedback about the structure of single donor cells in the living eye over a period of months, including evaluation of unfavorable aspects of the transplant environment, such as loss of a single donor cell. Other features of the transplanted photoreceptors that we imaged, such as neuronal

processes within an ablated retina (Figures 4 and S2) warrant further study and may provide insight into neurite formation after photoreceptor transplantation. Future study could also include 3D *in vivo* imaging of donor cells in which single cells could be imaged at multiple focal planes. Such three-dimensional volumetric imaging would be useful in exploring experimental manipulations to optimize the formation of functional synaptic connections. With sufficient lateral and axial resolution, FAOSLO would also permit the comparison of *in vivo* imaging data to the gold standard technique for retinal implants, immunohistochemistry, and would allow for the identification of each imaged cell. This approach may enable the development of a noninvasive means of detecting migration and integration of donor cells into the host retina, which would be a major advance to cell transplantation studies. The combination of *in vivo* single-cell tracking with the future development of fluorescent markers for features, such as glucose level, PH, etc., may allow for the detailed assessment and manipulation of both the recipient retina and donor cells after transplantation.

EXPERIMENTAL PROCEDURES

All animal procedures were approved by the institutional animal care and use committee of the University of Rochester (PHS assurance number: D16-00188(A3292-01)) and conducted in accordance with the ARVO statement for the use of animals in ophthalmic and vision research. Table S1 summarizes the details of transplantation experiments.

Retinal Differentiation of the CRX$^{+/tdTomato}$ hESCs

A previously described CRX$^{+/tdTomato}$ hESC line was used for these studies (Phillips et al., 2018), and was differentiated to a retinal cell fate using established methods (Meyer et al., 2011; Phillips et al., 2018; Zhong et al., 2014). In brief, ROs were generated and isolated at day 20. These ROs contained all retinal neurons; however, the majority of the cells were CRX+ photoreceptors, which were robustly and specifically labeled with tdTomato in this cell line (Phillips et al., 2018). This fluorescent reporter cell line can be used to identify all post-mitotic photoreceptors at all stages of differentiation, from precursors to fully mature photoreceptors (Phillips et al., 2018). ROs were differentiated for 2.5 to 3.5 months (Table S1), when photoreceptors within ROs were primarily at the precursor stage and were the major cell type present. Before surgery, ROs were dissociated with papain (Worthington Biochemical) to facilitate single-cell imaging with adaptive optics after transplantation. Cells from completely dissociated ROs were counted ($\geq$95% viable) and resuspended in Hank's balanced salt solution without calcium and magnesium (Gibco) for injection.

Subretinal Transplantation

Photoreceptors from CRX$^{+/tdTomato}$ hESCs between 74 and 106 days post differentiation were transplanted via subretinal injection into 5 eyes of 5 monkeys (3 blebs in non-lesioned retinas and 3 blebs in laser-lesioned retinas). The subretinal transplantation procedures for all monkeys are fully described in Note S1.

Monkey Model of Photoreceptor Ablation Using an Ultrafast Laser and Adaptive Optics

A 730-nm ultrafast laser beam (Mai Tai XF-1 with DeepSee attachment, Spectra-Physics, Santa Clara, CA), which emitted short pulses of light (55 fs) with a repetition rate of 80 MHz was focused on the ONL through adaptive optics to create localized lesions in the photoreceptor layer. To create these lesions, an AOSLO system designed for two-photon excited fluorescence imaging in nonhuman primates was used, which has been described previously (Hunter et al., 2011; Sharma et al., 2016). A grid pattern of multiple non-overlapping lesions (6 exposures in monkey 4 and 12 exposures in monkey 5) at the perifovea was created to cover a larger area using laser powers in the range of 90–120 mW for 106 ms. The laser beam was scanned at a frame rate of 22.5 Hz over retinal location of 0.79° × 0.87° for each exposure. The morphology of laser lesions was assessed using *in vivo* imaging modalities (AOSLO, SLO, and OCT) for 1 month before each transplantation.

Laser Lesions in Nonhuman Primates Using a CW Laser

Five laser lesions (each 200 μm) were made in one monkey within less than ±3° of the fovea center using a Coherent Novus Omni laser. The wavelength used was 647 nm and the laser power was 200 mW for 0.02 s. The morphology of lesions was assessed with *in vivo* imaging modalities (OCT, AOSLO, and SLO) before transplantation. The transplantation outcome using this model is summarized in Figure S1.

FAOSLO Imaging

Details regarding the design and use of an FAOSLO system for primate imaging at the University of Rochester have been described previously (Gray et al., 2006). In brief, under a combination of ketamine (5–20 mg/kg), midazolam (0.25 mg/kg), and glycopyrrolate (0.017 mg/kg), and maintained on 1%–3% inspired isoflurane anesthesia, the macaque was secured in a stereotaxic device and aligned to the exit pupil of the FAOSLO. During anesthesia, heart rate, electrocardiogram, blood oxygenation, and respiratory rate were continuously monitored. Pupils were dilated and accommodation arrested using 1–2 drops each of phenylephrine hydrochloride (2.5%; Akorn, IL) and tropicamide (1%; Akorn). The eye was held open with a lid retractor and a lubricated permeable contact lens with genteal (Alcon, Fort Worth, USA) fitted to protect the cornea and correct refractive error. To limit random large ocular drift, animals were paralyzed with vecuronium (60 μg/kg/h), and at the end of the imaging session neostigmine (0.05 mg/kg) and glycopyrrolate (0.01 mg/kg) were used to reverse anesthesia. The duration of each imaging session was 6 h limited to one session per week. We recorded from two imaging channels simultaneously: a confocal NIR reflectance image of the photoreceptor cone mosaic, using a 796-nm superluminescent diode; and a fluorescence image using 561 nm excitation. In monkeys 1 and 2, emission was detected using a 630/92-nm emission filter to maximize signal detection, and a 1.5 airy disk pinhole. In subsequent

animals a 590/20-nm emission filter (MDF-TOM filter; Thorlabs) was used to increase tdTomato specificity, with a 2 airy disk pinhole. The two imaging detectors were photomultiplier tubes for both NIR reflectance channel (H7422-40) and the fluorescence channel (H7422-50; Hamamatsu). An additional light source (840 nm) together with a Hartmann-Shack wavefront sensor was used to detect wavefront aberrations that were corrected with a deformable mirror. The intensities of the imaging lights at the pupil plane were 20–40 μW (561 nm), 250 μW (790 nm), and 30–40 μW (840 nm). The field of view for imaging was: M1, 2.6° × 3.4°; M2, 2.6° × 3.4°; M3, 2° × 2°; M4 and M5, 1.9° × 1.9°).

Image Registration in AOSLO

The existence of eye motion, even in the anesthetized and paralyzed macaque, required us to register the recorded videos to create a final still image. We used custom dual-image registration software (Yang et al., 2014) to align thousands of individual frames into a single high signal-to-noise ratio integrated image. The software used the motion trace of a simultaneously obtained high signal-to-noise ratio NIR reflectance image to register a low SNR fluorescence video.

Conventional SLO and Spectral-Domain OCT

To obtain low-resolution information about transplanted cells and retinal health over a larger retinal area, multiple imaging modalities, including OCT and SLO (Heidelberg SPECTRALIS, Germany) were used. Recipient monkeys were imaged before and every 2 weeks after transplant, beginning 1 week after transplantation of donor cells. For imaging, the monkey was laid on an imaging cart while the head was supported by a chinrest. OCT scans of transplanted eyes were acquired with 92 B-scans centered on the location of the subretinal bleb. Ketamine (6 mg/kg) and 0.15 mg/kg medetomidine were used for anesthesia and the eyes were dilated with 1–2 drops each of phenylephrine hydrochloride (2.5%; Akorn) and tropicamide (1%; Akorn). Eyelid specula were used to keep the eyelids open. We used both 488-nm and near-IR excitation for SLO imaging. In monkeys 2 and 3, the eyes were imaged immediately after transplantation to assess the quality of the subretinal bleb. Once complete, anesthesia was reversed by an intramuscular injection of 0.2 mg/kg antisedan.

Quantification of the Transplanted Cell Area and Counting Single Cells

Over the entire tracking period, the total number of single cells at different retinal locations within six blebs in five monkeys (M1-M5) was counted using FAOSLO imaging. We then calculated the percentage of single cells with neurites at each time point. To measure the area of fluorescent cells, first a region of interest was selected around both the cell clusters and single cells at each time point post transplantation and then the area was measured using ImageJ.

Immunosuppression

The list of immunosuppressant drugs used in each animal is listed in Table S1 and the details about the procedure are described in Note S2.

Immunohistochemistry

Transplanted eyes were fixed in 4% paraformaldehyde in phosphate-buffered saline (PBS). Eyes were then cryoprotected in 30% sucrose, embedded in OCT, and cryosectioned at ~30 μm. Immunohistochemistry was performed as described previously (Meyer et al., 2009; Phillips et al., 2012). Primary antibodies and dilutions are listed in Table S2. In brief, sections were first blocked for 1 h incubated in 10% normal donkey serum, 0.5% Triton X, and 5% bovine serum albumin in PBS at room temperature. Sections were incubated in primary antibodies overnight at 4°C, followed by secondary incubation (1:500) for 30 min at room temperature. Following washes, slides were coverslipped with Prolong Gold with DAPI and imaged on a confocal microscope.

Statistical Analysis

All values were expressed as mean ± standard error. The data were analyzed using a non-parametric Mann-Whitney U test. A p value of <0.05 was considered to be statistically significant. The labels used in the graphs are *$p < 0.05$ and **$p < 0.01$.

SUPPLEMENTAL INFORMATION

Supplemental Information can be found online at https://doi.org/10.1016/j.stemcr.2020.06.019.

AUTHOR CONTRIBUTIONS

E.A. conducted AOSLO imaging of transplanted cells in lesioned animals, data analysis, co-wrote the original draft, and assisted with creating laser lesions. M.J.P. co-wrote the original draft, performed immunohistochemical examination and cell preparation. J.E.McG. performed AOSLO imaging of transplanted cells in monkeys with non-lesioned retinas, and data analysis. D.A.D. performed surgery for subretinal transplantation and assisted with CW laser lesions. J.M.S. and B.B. assisted with animal care, surgical instrumentation, and conventional SLO/OCT imaging. K.R.D. assisted with creating ultrafast laser lesions. L.D.J., K.L.N., S.A.S., and A.L.L. produced and grew cells for transplantation and assisted with cryo-sectioning and immunolabeling. J.J.H., W.H.M., D.M.G., and D.R.W. conceived the project and acquired funding. All authors were involved in designing the experiments and writing the paper.

CONFLICTS OF INTEREST

D.M.G. and M.J.P. have an ownership interest in Opsis Therapeutics LLC, which has licensed the technology to generate 3D ROs from pluripotent stem cell sources reported in this publication. D.R.W. is a coinventor on a patent with the University of Rochester related to the fluorescence adaptive optics imaging methods used in this paper.

ACKNOWLEDGMENTS

We thank the Division of Comparative Medicine (DCM) and services provided by the staff and technicians in the vivarium animal housing area. Research reported in this study was supported by the National Eye Institute of the NIH under awards no. U01 EY025497–Audacious Goals Initiative, no. U54HD090256 core

grant to the Waisman Center, and no. P30 EY001319 core grant, and by an Unrestricted Grant to the University of Rochester Department of Ophthalmology from Research to Prevent Blindness, New York, Retina Research Foundation Emmett A. Humble Directorship to David Gamm, the Sandra Lemke Trout Chair in Eye Research to David Gamm, the Muskingum County Community Foundation and the Carl Marshall Reeves and Mildred Almen Reeves Foundation. We thank Selia Soto, Ruchira Singh, and Richard Libby for technical assistance with cell preparation. We also thank Amber Walker for her assistance with monkey imaging and surgery; Sarah Mack, Thurma McDaniel, and Tracy Bubel for their assistance with preparing fixative solutions, euthanasia, and histology; William Fischer for his assistance with fundus imaging, and Samuel Sullivan for his assistance with surgery.

Received: November 26, 2019
Revised: June 19, 2020
Accepted: June 22, 2020
Published: July 23, 2020

REFERENCES

Barber, A.C., Hippert, C., Duran, Y., West, E.L., Bainbridge, J.W., Warre-Cornish, K., Luhmann, U.F., Lakowski, J., Sowden, J.C., Ali, R.R., and Pearson, R.A. (2013). Repair of the degenerate retina by photoreceptor transplantation. Proc. Natl. Acad. Sci. U S A *110*, 354–359.

Busskamp, V., Picaud, S., Sahel, J.A., and Roska, B. (2012). Optogenetic therapy for retinitis pigmentosa. Gene Ther. *19*, 169.

Chao, J.R., Lamba, D.A., Klesert, T.R., La Torre, A., Hoshino, A., Taylor, R.J., Jayabalu, A., Engel, A.L., Khuu, T.H., Wang, R.K., and Neitz, M. (2017). Transplantation of human embryonic stem cell-derived retinal cells into the subretinal space of a non-human primate. Transl. Vis. Sci. Technol. *6*, 4.

da Cruz, L., Fynes, K., Georgiadis, O., Kerby, J., Luo, Y.H., Ahmado, A., Vernon, A., Daniels, J.T., Nommiste, B., Hasan, S.M., and Gooljar, S.B. (2018). Phase 1 clinical study of an embryonic stem cell-derived retinal pigment epithelium patch in age-related macular degeneration. Nat. Biotechnol. *36*, 328.

Dhakal, K.R., Walters, S., McGregor, J.E., Schwarz, C., Strazzeri, J.M., Aboualizadeh, E., Bateman, B., Huxlin, K.R., Hunter, J.J., Williams, D.R., and Merigan, W.H. (2020). Localized photoreceptor ablation using femtosecond pulses focused with adaptive optics. Transl. Vis. Sci. Technol. *9*, 16.

Gasparini, S.J., Llonch, S., Borsch, O., and Ader, M. (2018). Transplantation of photoreceptors into the degenerative retina: current state and future perspectives. Prog. Retin. Eye Res. *69*, 1–37.

Ghezzi, D. (2015). Retinal prostheses: progress toward the next generation implants. Front. Neurosci. *9*, 290.

Gray, D.C., Merigan, W., Wolfing, J.I., Gee, B.P., Porter, J., Dubra, A., Twietmeyer, T.H., Ahmad, K., Tumbar, R., Reinholz, F., and Williams, D.R. (2006). In vivo fluorescence imaging of primate retinal ganglion cells and retinal pigment epithelial cells. Opt. Express *14*, 7144–7158.

Hunter, J.J., Masella, B., Dubra, A., Sharma, R., Yin, L., Merigan, W.H., Palczewska, G., Palczewski, K., and Williams, D.R. (2011). Images of photoreceptors in living primate eyes using adaptive optics two-photon ophthalmoscopy. Biomed. Opt. Express *2*, 139–148.

Jain, A., Blumenkranz, M.S., Paulus, Y., Wiltberger, M.W., Andersen, D.E., Huie, P., and Palanker, D. (2008). Effect of pulse duration on size and character of the lesion in retinal photocoagulation. Arch. Ophthalmol. *126*, 78–85.

Jayakody, S.A., Gonzalez-Cordero, A., Ali, R.R., and Pearson, R.A. (2015). Cellular strategies for retinal repair by photoreceptor replacement. Prog. Retin. Eye Res. *46*, 31–66.

Kashani, A.H., Lebkowski, J.S., Rahhal, F.M., Avery, R.L., Salehi-Had, H., Dang, W., Lin, C.M., Mitra, D., Zhu, D., Thomas, B.B., and Hikita, S.T. (2018). A bioengineered retinal pigment epithelial monolayer for advanced, dry age-related macular degeneration. Sci. Transl. Med. *10*, eaao4097.

Lakowski, J., Welby, E., Budinger, D., Di Marco, F., Di Foggia, V., Bainbridge, J.W., Wallace, K., Gamm, D.M., Ali, R.R., and Sowden, J.C. (2018). Isolation of human photoreceptor precursors via a cell surface marker panel from stem cell-derived retinal organoids and fetal retinae. Stem Cells *36*, 709–722.

McGill, T.J., Stoddard, J., Renner, L.M., Messaoudi, I., Bharti, K., Mitalipov, S., Lauer, A., Wilson, D.J., and Neuringer, M. (2018). Allogeneic iPSC-derived RPE cell graft failure following transplantation into the subretinal space in nonhuman primates. Invest. Ophthalmol. Vis. Sci. *59*, 1374–1383.

Meyer, J.S., Shearer, R.L., Capowski, E.E., Wright, L.S., Wallace, K.A., McMillan, E.L., Zhang, S.C., and Gamm, D.M. (2009). Modeling early retinal development with human embryonic and induced pluripotent stem cells. Proc. Natl. Acad. Sci. U S A *106*, 16698–16703.

Meyer, J.S., Howden, S.E., Wallace, K.A., Verhoeven, A.D., Wright, L.S., Capowski, E.E., Pinilla, I., Martin, J.M., Tian, S., Stewart, R., and Pattnaik, B. (2011). Optic vesicle-like structures derived from human pluripotent stem cells facilitate a customized approach to retinal disease treatment. Stem Cells *29*, 1206–1218.

Moshiri, A., Chen, R., Kim, S., Harris, R.A., Li, Y., Raveendran, M., Davis, S., Liang, Q., Pomerantz, O., Wang, J., and Garzel, L. (2019). A nonhuman primate model of inherited retinal disease. J. Clin. Invest. *129*, 863–874.

Ortin-Martinez, A., Tsai, E.L.S., Nickerson, P.E., Bergeret, M., Lu, Y., Smiley, S., Comanita, L., and Wallace, V.A. (2017). A reinterpretation of cell transplantation: GFP transfer from donor to host photoreceptors. Stem Cells *35*, 932–939.

Pearson, R.A., Barber, A.C., West, E.L., MacLaren, R.E., Duran, Y., Bainbridge, J.W., Sowden, J.C., and Ali, R.R. (2010). Targeted disruption of outer limiting membrane junctional proteins (Crb1 and ZO-1) increases integration of transplanted photoreceptor precursors into the adult wild-type and degenerating retina. Cell Transplant. *19*, 487–503.

Pearson, R.A., Gonzalez-Cordero, A., West, E.L., Ribeiro, J.R., Aghaizu, N., Goh, D., Sampson, R.D., Georgiadis, A., Waldron, P.V., Duran, Y., and Naeem, A. (2016). Donor and host photoreceptors engage in material transfer following transplantation of post-mitotic photoreceptor precursors. Nat. Commun. *7*, 13029.

Peterson, S.M., McGill, T.J., Puthussery, T., Stoddard, J., Renner, L., Lewis, A.D., Colgin, L.M., Gayet, J., Wang, X., Prongay, K., and Cullin, C. (2019). Bardet-Biedl syndrome in rhesus macaques: a nonhuman primate model of retinitis pigmentosa. Exp. Eye Res. *189*, 107825.

Phillips, M.J., Wallace, K.A., Dickerson, S.J., Miller, M.J., Verhoeven, A.D., Martin, J.M., Wright, L.S., Shen, W., Capowski, E.E., Percin, E.F., and Perez, E.T. (2012). Blood-derived human iPS cells generate optic vesicle-like structures with the capacity to form retinal laminae and develop synapses. Invest. Ophthalmol. Vis. Sci. *53*, 2007–2019.

Phillips, M.J., Perez, E.T., Martin, J.M., Reshel, S.T., Wallace, K.A., Capowski, E.E., Singh, R., Wright, L.S., Clark, E.M., Barney, P.M., and Stewart, R. (2014). Modeling human retinal development with patient-specific induced pluripotent stem cells reveals multiple roles for visual system homeobox 2. Stem Cells *32*, 1480–1492.

Phillips, M.J., Jiang, P., Howden, S., Barney, P., Min, J., York, N.W., Chu, L.F., Capowski, E.E., Cash, A., Jain, S., and Barlow, K. (2018). A novel approach to single cell RNA-sequence analysis facilitates in silico gene reporting of human pluripotent stem cell-derived retinal cell types. Stem Cells *36*, 313–324.

Regenberg, A., Mathews, D.J., Blass, D.M., Bok, H., Coyle, J.T., Duggan, P., Faden, R., Finkel, J., Gearhart, J.D., Hillis, A., and Hoke, A. (2009). The role of animal models in evaluating reasonable safety and efficacy for human trials of cell-based interventions for neurologic conditions. J. Cereb. Blood Flow Metab. *29*, 1–9.

Rossi, E.A., Granger, C.E., Sharma, R., Yang, Q., Saito, K., Schwarz, C., Walters, S., Nozato, K., Zhang, J., Kawakami, T., and Fischer, W. (2017). Imaging individual neurons in the retinal ganglion cell layer of the living eye. Proc. Natl. Acad. Sci. U S A *114*, 586–591.

Santos-Ferreira, T., Llonch, S., Borsch, O., Postel, K., Haas, J., and Ader, M. (2016). Retinal transplantation of photoreceptors results in donor-host cytoplasmic exchange. Nat. Commun. *7*, 13028.

Santos-Ferreira, T.F., Borsch, O., and Ader, M. (2017). Rebuilding the missing part—a review on photoreceptor transplantation. Front. Syst. Neurosci. *10*, 105.

Sharma, R., Schwarz, C., Williams, D.R., Palczewska, G., Palczewski, K., and Hunter, J.J. (2016). In vivo two-photon fluorescence kinetics of primate rods and cones. Invest. Ophthalmol. Vis. Sci. *57*, 647–657.

Sharma, R., Khristov, V., Rising, A., Jha, B.S., Dejene, R., Hotaling, N., Li, Y., Stoddard, J., Stankewicz, C., Wan, Q., and Zhang, C. (2019). Clinical-grade stem cell-derived retinal pigment epithelium patch rescues retinal degeneration in rodents and pigs. Sci. Transl. Med. *11*, eaat5580.

Shirai, H., Mandai, M., Matsushita, K., Kuwahara, A., Yonemura, S., Nakano, T., Assawachananont, J., Kimura, T., Saito, K., Terasaki, H., and Eiraku, M. (2016). Transplantation of human embryonic stem cell-derived retinal tissue in two primate models of retinal degeneration. Proc. Natl. Acad. Sci. U S A *113*, E81–E90.

Singh, M.S., Balmer, J., Barnard, A.R., Aslam, S.A., Moralli, D., Green, C.M., Barnea-Cramer, A., Duncan, I., and MacLaren, R.E. (2016). Transplanted photoreceptor precursors transfer proteins to host photoreceptors by a mechanism of cytoplasmic fusion. Nat. Commun. *7*, 13537.

Singh, R., Cuzzani, O., Binette, F., Sternberg, H., West, M.D., and Nasonkin, I.O. (2018). Pluripotent stem cells for retinal tissue engineering: current status and future prospects. Stem Cell Rev. Rep. *14*, 463–483.

Strazzeri, J.M., Hunter, J.J., Masella, B.D., Yin, L., Fischer, W.S., DiLoreto, D.A., Jr., Libby, R.T., Williams, D.R., and Merigan, W.H. (2014). Focal damage to macaque photoreceptors produces persistent visual loss. Exp. Eye Res. *119*, 88–96.

Thompson, S., Blodi, F.R., Lee, S., Welder, C.R., Mullins, R.F., Tucker, B.A., Stasheff, S.F., and Stone, E.M. (2014). Photoreceptor cells with profound structural deficits can support useful vision in mice. Invest. Ophthalmol. Vis. Sci. *55*, 1859–1866.

Tu, H.Y., Watanabe, T., Shirai, H., Yamasaki, S., Kinoshita, M., Matsushita, K., Hashiguchi, T., Onoe, H., Matsuyama, T., Kuwahara, A., and Kishino, A. (2019). Medium- to long-term survival and functional examination of human iPSC-derived retinas in rat and primate models of retinal degeneration. EBioMedicine *39*, 562–574.

Vogel, A., and Venugopalan, V. (2003). Mechanisms of pulsed laser ablation of biological tissues. Chem. Rev. *103*, 577–644.

West, E.L., Pearson, R.A., Tschernutter, M., Sowden, J.C., MacLaren, R.E., and Ali, R.R. (2008). Pharmacological disruption of the outer limiting membrane leads to increased retinal integration of transplanted photoreceptor precursors. Exp. Eye Res. *86*, 601–611.

Williams, D.R. (2011). Imaging single cells in the living retina. Vis. Res. *51*, 1379–1396.

Yang, Q., Zhang, J., Nozato, K., Saito, K., Williams, D.R., Roorda, A., and Rossi, E.A. (2014). Closed-loop optical stabilization and digital image registration in adaptive optics scanning light ophthalmoscopy. Biomed. Opt. Express *5*, 3174–3191.

Zhang, S.C., Wernig, M., Duncan, I.D., Brüstle, O., and Thomson, J.A. (2001). In vitro differentiation of transplantable neural precursors from human embryonic stem cells. Nat. Biotechnol. *19*, 1129.

Zhong, X., Gutierrez, C., Xue, T., Hampton, C., Vergara, M.N., Cao, L.H., Peters, A., Park, T.S., Zambidis, E.T., Meyer, J.S., and Gamm, D.M. (2014). Generation of three-dimensional retinal tissue with functional photoreceptors from human iPSCs. Nat. Commun. *5*, 4047.